Front. Med. 2019, 13(5): 602–609
https://doi.org/10.1007/s11684-019-0704-x

RESEARCH ARTICLE

PET imaging on neurofunctional changes after optogenetic stimulation in a rat model of panic disorder

Xiao He[1,2,3,*], Chentao Jin[1,2,3,*], Mindi Ma[1,2,3,*], Rui Zhou[1,2,3], Shuang Wu[1,2,3], Haoying Huang[1,2,3], Yuting Li[1,2,3], Qiaozhen Chen[2,4], Mingrong Zhang (✉)[5], Hong Zhang (✉)[1,2,3], Mei Tian (✉)[1,2,3]

[1]Department of Nuclear Medicine and Medical PET Center, The Second Hospital of Zhejiang University School of Medicine, Hangzhou 310009, China; [2]Key Laboratory of Medical Molecular Imaging of Zhejiang Province, Hangzhou 310009, China; [3]Institute of Nuclear Medicine and Molecular Imaging, Zhejiang University, Hangzhou 310009, China; [4]Department of Psychiatry, The Second Hospital of Zhejiang University School of Medicine, Hangzhou 310009, China; [5]Department of Advanced Nuclear Medicine Sciences, National Institute of Radiological Sciences, National Institutes for Quantum and Radiological Science and Technology, Anagawa 4-9-1, Inage-ku, Chiba, 263-8555, Japan

Abstract **Panic disorder (PD) is an acute paroxysmal anxiety disorder with poorly understood pathophysiology. The dorsal periaqueductal gray (dPAG) is involved in the genesis of PD. However, the downstream neurofunctional changes of the dPAG during panic attacks have yet to be evaluated *in vivo*. In this study, optogenetic stimulation to the dPAG was performed to induce panic-like behaviors, and *in vivo* positron emission tomography (PET) imaging with ^{18}F-flurodeoxyglucose (^{18}F-FDG) was conducted to evaluate neurofunctional changes before and after the optogenetic stimulation. Compared with the baseline, post-optogenetic stimulation PET imaging demonstrated that the glucose metabolism significantly increased ($P < 0.001$) in dPAG, the cuneiform nucleus, the cerebellar lobule, the cingulate cortex, the alveus of the hippocampus, the primary visual cortex, the septohypothalamic nucleus, and the retrosplenial granular cortex but significantly decreased ($P < 0.001$) in the basal ganglia, the frontal cortex, the forceps minor corpus callosum, the primary somatosensory cortex, the primary motor cortex, the secondary visual cortex, and the dorsal lateral geniculate nucleus. Taken together, these data indicated that *in vivo* PET imaging can successfully detect downstream neurofunctional changes involved in the panic attacks after optogenetic stimulation to the dPAG.**

Keywords panic disorder (PD); positron emission tomography (PET); optogenetics; dorsal periaqueductal gray (dPAG)

Introduction

Anxiety disorder is a prevalent mental disorder affecting 20% of individuals over a lifetime [1]. Panic disorder (PD), a type of the anxiety disorder defined by the presence of recurrent and unexpected panic attacks (PAs), is rarely investigated. Several functional magnetic resonance imaging (fMRI) and positron emission tomography (PET) studies on PD patients have reported increased activity in the midbrain periaqueductal gray matter (PAG), the amygdala, and the anterior cingulate cortex [2–5]. Emerging evidence has implicated that the dorsal periaqueductal gray matter (dPAG) is involved in the genesis of PAs. Electrical stimulation of the dPAG in healthy humans evokes emotional and autonomic responses that resemble spontaneously occurring PAs in PD patients [6]. Further studies using a rodent model revealed that stimulation of the dPAG induces defensive behaviors (freezing and escape) [7] and neurovegetative reactions (hypertension, tachycardia and tachypnea) [8]. These responses in animal model resemble the PAs occurring in healthy humans with dPAG stimulation or in PD patients [9,10]. So far, the dPAG stimulation approach has been recognized as a common model for preclinical PD studies.

Until now, PD animal models are mainly established by chemical and electrical stimulation of the dPAG [11–16]. However, these two methods could not stimulate the dPAG

Received April 2, 2019; accepted June 12, 2019

Correspondence: Mei Tian, meitian@zju.edu.cn;
Hong Zhang, hzhang21@zju.edu.cn;
Mingrong Zhang, zhang.ming-rong@qst.go.jp

*These authors contribute equally to this study.

precisely because of poor time response and low specificity. Optogenetic stimulation, an emerging neuromodulation technology that utilizes light pulses to trigger neural activity *in vivo*, is a powerful and precise method to induce panic-like behaviors [17].

Traditionally, the effects of dPAG stimulation are evaluated by c-Fos (a neuroactivity marker) immunohistochemistry [18,19], which is invasive and at the *ex vivo* level. Therefore, we hypothesized that PET, an *in vivo* and non-invasive imaging technique, is suitable in screening whole-brain activation patterns during PAs. Here, we used PET imaging to map the downstream neurofunctional changes after precise optogenetic stimulation to the dPAG and to establish an optogenetic-PET paradigm for understanding the contribution of specific brain regions to PD.

Materials and methods

Animals

Male Sprague Dawley rats (body weight, 250–300 g) were kept under standard laboratory conditions with food and water ad libitum. The animal experiment was approved by the Institutional Animal Care and Use Committee at Zhejiang University School of Medicine (Protocol No. ZJU201407-1-02-067).

Virus injection and fiber optic cannula implantation

Adeno-associated virus (AAV) carrying photosensitive gene channelrhodopsi-2 (ChR2) with mCherry fluorescent marker and CaMKIIα promoter (AAV2/9-CaMKIIα-ChR2-mCherry, $ChR2^+$) or AAV2/9-CaMKIIα-mCherry ($ChR2^-$) were prepared as previously described [17]. Rats were randomly divided into either the experimental group ($ChR2^+$, $n = 9$) or the control group ($ChR2^-$, $n = 9$). $ChR2^+$ or $ChR2^-$ virus (300 nL) was infused into the dPAG at a flow rate of 100 nL/min (coordinates: AP: −7.25 mm, ML: 1.8 mm from bregma; DV: −5.3 mm from the skull surface angled 16° to the midline) by using stereotaxic guidance. Two weeks after the virus injection, the rats were implanted with a fiber optic cannula (200 μm, NA = 0.37) at 0.3 mm dorsally to the site of virus injection and then kept for another week for complete recovery (Fig. 1A).

Optogenetic stimulation and PET imaging

Optogenetic stimulation was performed as previously described [20]. In brief, the rats were connected to the optical fiber via the implanted cannula and placed in a Plexiglas box (dimensions 52 cm × 38 cm × 44 cm) to allow free movement. Then, optogenetic stimulation (50 Hz blue, 473 nm laser) was performed via the optical fiber for 30 min with 30 s intervals (30 s on/30 s off) to induce panic-like behaviors (details are provided in the supplementary materials).

Baseline and post-optogenetic stimulation ^{18}F-fluorodeoxyglucose (^{18}F-FDG) PET scans were performed on

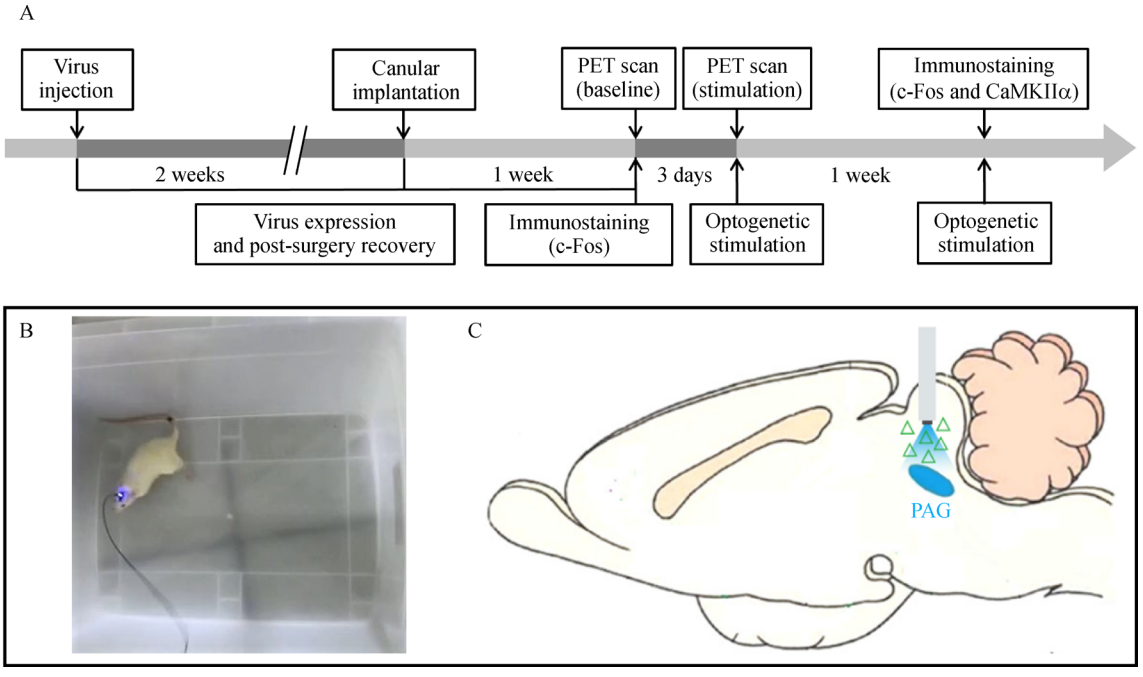

Fig. 1 Experimental design and the site of optogenetic stimulation. (A) PET scanning and optogenetic stimulation protocol. (B) Schematic showing panic-like defensive behaviors induced by 473 nm blue laser stimulation. (C) Schematic showing the site of target nucleus undergoing the laser stimulation.

the microPET R4 scanner (Siemens Medical Solutions) within an interval of 3 days [21].

Immunostaining

After 3 weeks of virus injection, a batch of rats (n = 3 in ChR2$^-$, n = 3 in ChR2$^+$) was sacrificed (without stimulation) for c-Fos immunostaining to evaluate the baseline neuronal activity of the dPAG. One week after the second PET scan (stimulation), another batch of rats (n = 4 in ChR2$^-$, n = 5 in ChR2$^+$) was sacrificed for c-Fos immunostaining to evaluate the effects of optogenetic stimulation on the neuronal activity of the dPAG and CaMKIIα immunostaining to examine the expression of ChR2-mCherry in excitatory neurons of the dPAG (Fig. 1A, details are provided in the supplementary materials). CaMKIIα and c-Fos positive cells were counted by using ImageJ software (NIH).

PET image and statistical analysis

PET images were analyzed by Statistical Parametric Mapping software. Paired t-tests were performed to evaluate regional metabolic differences between baseline and post-stimulation PET images. Statistical significance was determined when P value < 0.001 and cluster $K_e > 100$ [22].

To measure glucose metabolic changes in the dPAG following optogenetic stimulation, the region of interest (ROI) was drawn on PET images by using PMOD (v.3.902, PMOD Technologies Ltd.) software. The ^{18}F-FDG uptake of the dPAG was normalized to the whole brain (dPAG activity/whole-brain activity) [20]. Two-way repeated-measures ANOVA was used to compare glucose metabolic changes between the baseline and post-stimulation PET imaging.

Independent t-test was conducted to compare the number of c-Fos positive cells in the dPAG with or without the optogenetic stimulation. Data were presented as mean ± SEM, and $P < 0.05$ was considered significant. Pearson correlation analysis was performed to assess the relation between c-Fos expression and glucose metabolism (GluM) in the dPAG after optogenetic stimulation.

Results

Panic-like behaviors induced by precise optogenetic stimulation

We found obvious panic-like behaviors, such as galloping, jumping, and rotation, in the ChR2$^+$ rats after precise optogenetic stimulation to the excitatory neurons of dPAG but not in the ChR2$^-$ control (Fig. 1B and 1C, supplemental Videos 1 and 2).

Brain glucose utilization in response to optogenetic stimulation of the dPAG

In the ChR2$^+$ group, post-optogenetic stimulation PET images demonstrated that the ^{18}F-FDG accumulation significantly increased in the dPAG, the cuneiform nucleus, the cerebellar lobule, the cingulate cortex, the alveus of the hippocampus, the primary visual cortex, the septohypothalamic nucleus, and the retrosplenial granular cortex ($P < 0.001$ in each comparison) but decreased in the basal ganglia, the frontal cortex, the forceps minor corpus callosum, the primary somatosensory cortex, the primary motor cortex, the secondary visual cortex, and the dorsal lateral geniculate nucleus ($P < 0.001$ in each comparison) compared with the baseline (Table 1, Fig. 2A, and supplemental Fig. S1A). However, this widespread pattern was not found in the ChR2$^-$ control (supplemental Fig. S1B).

Furthermore, we performed ROI analysis of the dPAG to confirm the effects of optogenetic stimulation on the regional glucose accumulation. Compared with the baseline, the glucose metabolism in the dPAG significantly increased in the ChR2$^+$ group after optogenetic stimulation ($P < 0.001$), but a different phenomenon was observed in the ChR2$^-$ control. Additionally, the ChR2$^+$ group had significantly increased glucose metabolism in the dPAG after optogenetic stimulation compared with the ChR2$^-$ control ($P < 0.01$) (Fig. 2B and 2C).

ChR2 expression and fiber optic cannula implantation

Immunofluorescent results confirmed the appropriate expression of ChR2 and the precise implantation of the fiber optic cannula (Fig. 3A). Furthermore, CaMKIIα immunostaining tests verified the specificity and efficacy of AAV virus (ChR2$^+$ and ChR2$^-$) expression in the excitatory neurons of the dPAG (Fig. 3B and 3C).

C-Fos expression in the dPAG after optogenetic stimulation

After optogenetic stimulation, c-Fos expression ($P < 0.001$) significantly increased in the ChR2$^+$ group compared with the ChR2$^-$ control, whereas no significant difference was found between the ChR2$^+$ and ChR2$^-$ groups without the stimulation (Fig. 4A and 4B). Moreover, glucose metabolic changes in both ChR2$^+$ and ChR2$^-$ groups significantly correlated with the c-Fos expression in the dPAG after optogenetic stimulation (Fig. 4C).

Table 1 Significant metabolic changes after optogenetic stimulation of the dPAG (baseline vs. stimulation)

Brain region	Coordinate (mm)			K_e	T value	Z score	$P_{\text{uncorrected}}$
	x	y	z				
Increased							
Dorsal periaqueductal gray	1	5	−7	3051	15.66	4.27	<0.001
Cuneiform nucleus	−2	6	−8		7.83	3.46	<0.001
Cerebellar lobule	1	2	−13	1312	10.47	3.81	<0.001
Cingulate cortex	1	2	2	221	7.05	3.32	<0.001
Alveus of the hippocampus	−6	4	−7	1305	8.44	3.55	<0.001
Primary visual cortex	−4	2	−9		7.87	3.46	<0.001
Septohypothalamic nucleus	−1	6	0	962	18.40	4.45	<0.001
Retrosplenial granular cortex	0	2	−3	158	7.47	3.40	<0.001
Decreased							
Basal ganglia	3	5	2	1694	8.00	3.49	<0.001
Frontal cortex	4	4	4		8.04	3.49	<0.001
Forceps minor corpus callosum	−3	3	4	7173	19.35	4.50	<0.001
Primary somatosensory cortex	−5	5	1		16.93	4.36	<0.001
Primary motor cortex	−3	2	2		10.17	3.78	<0.001
Secondary visual cortex	−3	1	−5	890	14.61	4.20	<0.001
Dorsal lateral geniculate nucleus	3	4	−4	1073	11.95	3.97	<0.001

Discussion

In the present study, precise optogenetic stimulation to the excitatory neurons of dPAG induced panic-like behaviors, and the glucose metabolism significantly increased in the dPAG, the cuneiform nucleus, the cerebellar lobule, the cingulate cortex, the alveus of the hippocampus, the primary visual cortex, the septohypothalamic nucleus, and the retrosplenial granular cortex but decreased in the basal ganglia, the frontal cortex, the forceps minor corpus callosum, the primary somatosensory cortex, the primary motor cortex, the secondary visual cortex, and the dorsal lateral geniculate nucleus. Moreover, increased glucose metabolism in the dPAG was associated with the over-expression of c-Fos.

Glucose provides the fuel for physiologic brain function, including the generation of action potentials and post-synaptic potentials [23], which could reflect the changes in brain activity, both in laboratory animals and humans [20,24]. After optogenetic activation with ChR2, glucose accumulation (activation) increased in the region of stimulation and the downstream nuclei (via the direct or indirect excitatory projection) but decreased in the down-stream nuclei (via an increase in the activity of inhibitory circuits) [20]. To the best of our knowledge, this PET study is the first to evaluate glucose metabolic changes after precise optogenetic stimulation to the excitatory neurons of the dPAG.

Previously, chemical induction or electrical stimulation of dPAG was performed to induce intense symptoms of PAs in animal models [12,16]. However, compared with electrical and chemical methods, optogenetic techniques could avoid non-specific activation/inhibition with superior spatiotemporal resolution [25–27]. In the present study, we demonstrated that precise optogenetic stimulation to the excitatory neurons of dPAG could induce panic-like behaviors successfully. In addition, increased glucose metabolism was associated with c-Fos expression at the site of optogenetic stimulation of the dPAG. This result is consistent with the previous results on PET study in which optogenetic stimulation with ChR2 activated neurons in the region where light was delivered [20].

Increased glucose metabolism in the cuneiform nucleus after optogenetic stimulation of the dPAG was observed in our study, supporting that the cuneiform nucleus is the direct descending projection region of the dPAG [28,29]. The cuneiform nucleus is involved in organizing panic-like defensive behaviors, and chemical stimulation of this nucleus could induce freezing and escape behaviors in rodents [29]. Furthermore, a recent diffusion weighted imaging study on monkey and human demonstrated that the cuneiform nucleus could project to the sensorimotor territories of basal ganglia, which is decreased in glucose metabolism in our PET imaging results [30]. The basal ganglia's primary function is likely to control and regulate activities of the motor and premotor cortical areas so that voluntary movements can be performed smoothly [31].

Previous studies have also shown that PAG can descend into the cerebellum [32,33], which can mediate the

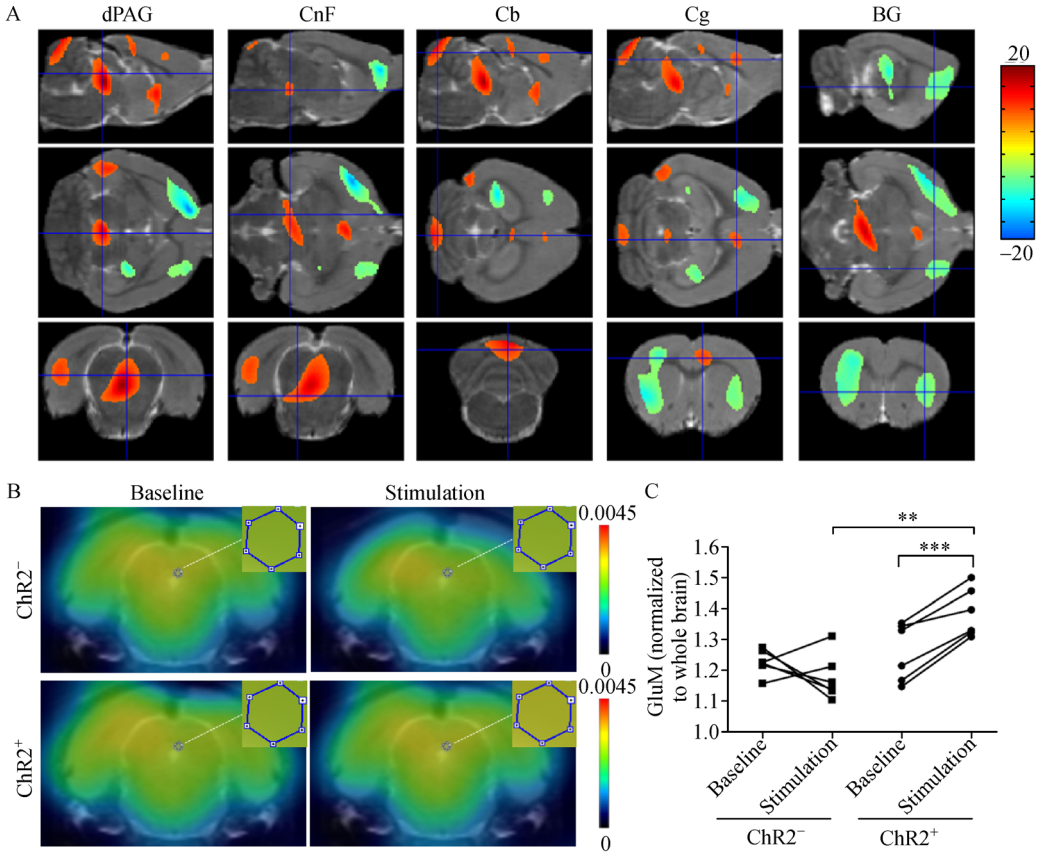

Fig. 2 *In vivo* ^{18}F-FDG PET images of the rat brain. (A) Representative sagittal (top), transverse (middle), and coronal (bottom) PET images demonstrated alternation of glucose metabolism in the dPAG, the cuneiform nucleus (CnF), cerebellar lobule (Cb), cingulate cortex (Cg), basal ganglia (BG) after dPAG stimulation ($n = 6$ in each group; $P < 0.001$). (B) ROI results showed glucose metabolism (GluM) in the region of stimulation. (C) Individual metabolic values (normalized to whole brain) in the dPAG cluster during the baseline and stimulation PET scans in the ChR2$^-$ (left) and ChR2$^+$ (right) groups ($n = 6$ in each group; ***$P < 0.001$, **$P < 0.01$).

preferential encoding of movement speed [34]. This result is in conjunction with the increased metabolic activity in the cerebellum lobe in our PET results. Clinically, patients with PD show increased regional cerebral blood flow within the anterior cingulate cortex during anticipatory anxiety [5,35]. Our results of increased glucose metabolism in the anterior cingulate cortex are in line with the above PET study. The anterior cingulate is involved in automatic attentional control as well as in response to selection and conflict monitoring, thus enabling rapid access to the motor system [36].

In the current study, increased glucose metabolism was observed in the alveus of the hippocampus that contains input and output pathways for the hippocampus, which is consistent with a study of PD patients using ^{18}F-FDG PET with lactate infusion stimulation [37]. Taking these pieces of evidence together, we assume that the hippocampus is involved in the complex panic behaviors. Conversely, glucose metabolism in the right inferior parietal and superior temporal areas presented no change in our animal study but decreased in the same areas in the PD patient study because of the difference of research subjects (rat vs. human) and type of stimulation (precise optogenetic stimulation vs. diffuse lactate provocation).

The panic animal model used in this study was established mainly based on criteria of behavior evaluation according to previous studies [14,15,17]. In future studies, we will use more physiologic parameters (such as heart rate, body temperature, micturition, and defecation) on the panic animal model for further investigating the mechanism of related neural circuits.

In summary, the approach of combining optogenetics and PET used in this study may identify the specific brain function patterns of panic-like behaviors in rats. Greater insights into the neural connectivity of brain regions involved in the PD may be gained by future PET studies that combine patch-clamp and viral tracing technologies in the same subjects. In addition, brain network analysis methods, such as dynamic causal modeling for optogenetic fMRI experiments [38], might also contribute to further PET studies in parameterizing causal relationships among regions of a distributed brain network.

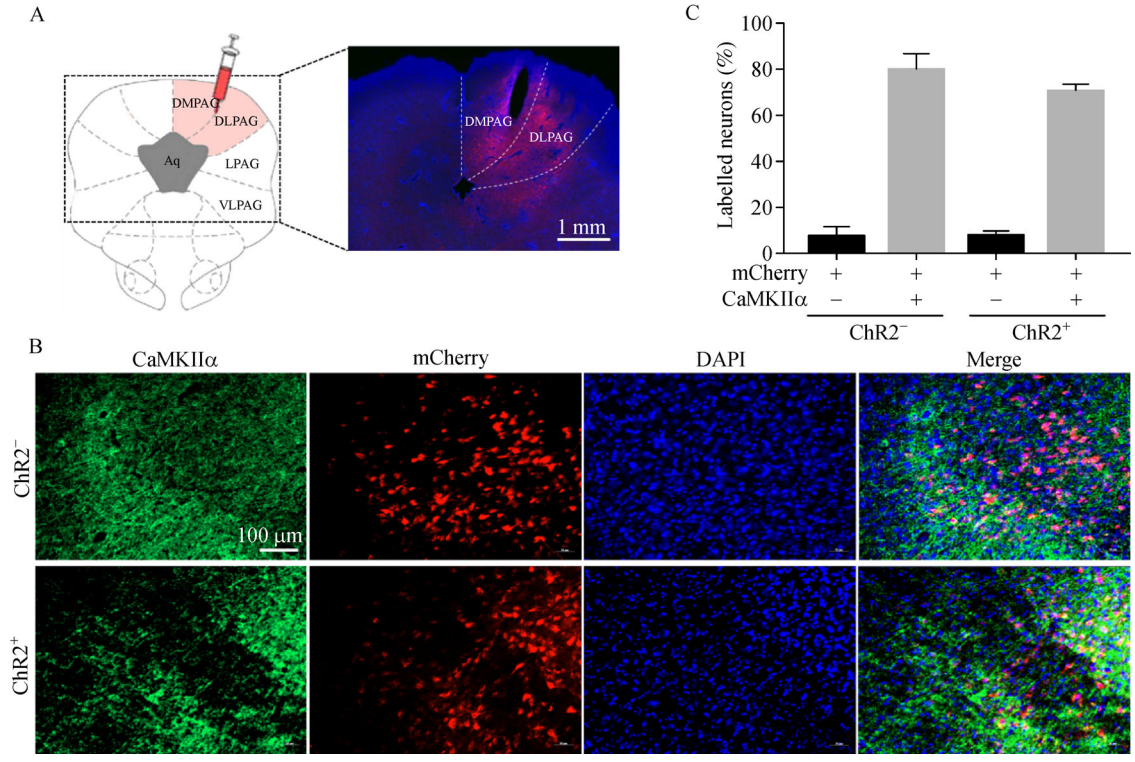

Fig. 3 Expression of AAV2/9-CaMKIIα-(ChR2)-mCherry in the excitatory neurons of dPAG. (A) Left: Diagrams showing the virus injection site in the dPAG. Right: Representative fluorescent images confirming the fiber position (the tract) and expression of ChR2 (the red mCherry signal) in the dPAG. (B) Representative immunofluorescent images showing the co-expression of CaMKIIα and mCherry in the ChR2$^-$ and ChR2$^+$ groups. (C) Quantification showed that CaMKIIα$^-$ and mCherry$^+$ cells were less than 8% of the total mCherry$^+$ neurons in each group. Meanwhile, mCherry$^+$ and CaMKIIα$^+$ cells were more than 70% of the total CaMKIIα$^+$ neurons in each group (n = 4 in ChR2$^-$, n = 5 in ChR2$^+$).

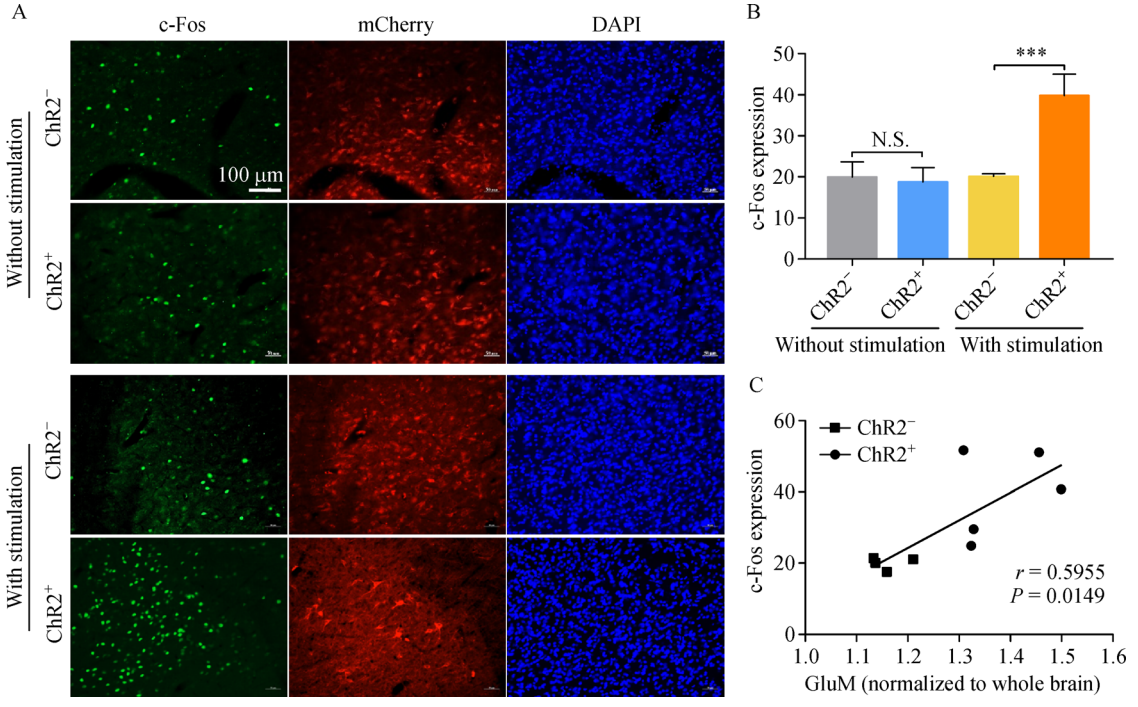

Fig. 4 Expression of c-Fos in the dPAG with or without stimulation. (A) Representative immunofluorescent images showed expression of c-Fos with or without stimulation in the ChR2$^-$ and ChR2$^+$ groups. (B) Quantification of c-Fos positive cells in the dPAG with (n = 4 in ChR2$^-$, n = 5 in ChR2$^+$; ***$P < 0.001$) or without (n = 3 in each group; N.S., no significance) stimulation. (C) Correlation between c-Fos expression and GluM in the dPAG after stimulation (n = 4 in ChR2$^-$, n = 5 in ChR2$^+$; r = 0.5955, P = 0.0149).

Conclusions

^{18}F-FDG PET could map neurofunctional changes after optogenetic stimulation to the dPAG during PAs. This optogenetic-PET paradigm could help us understand the role of specific brain regions in the pathogenesis of PD. Future studies are required to better delineate the contribution of the dPAG in PD and its functional connectivity with other brain regions.

Acknowledgements

We thank Prof. Binggui Sun for providing devices and laboratory space in virus injection, Binbin Nie for technical support in Statistical Parametric Mapping analysis and Qianyun Liu (Hopstem Biotechnology LLC) for technical support on immunostaining. Help from the Zhejiang University Intelligence Convergence was greatly appreciated. This work was supported by grants from the National Natural Science Foundation of China (No. 81425015), the National Key Research and Development Program of China (No. 2016YFA0100900), the National Natural Science Foundation of China (Nos. 81725009, 81761148029, and 81571711), and Zhejiang University K.P. Chao's High Technology Development Foundation.

Compliance with ethics guidelines

Xiao He, Chentao Jin, Mindi Ma, Rui Zhou, Shuang Wu, Haoying Huang, Yuting Li, Qiaozhen Chen, Mingrong Zhang, Hong Zhang, and Mei Tian declare that they have no conflicts of interests associated with this study. All animal protocols were approved by the Institutional Animal Care and Use Committee at Zhejiang University School of Medicine.

Electronic Supplementary Material Supplementary material is available in the online version of this article at https://doi.org/10.1007/s11684-019-0704-x and is accessible for authorized users.

References

1. Meier SM, Deckert J. Genetics of anxiety disorders. Curr Psychiatry Rep 2019; 21(3): 16
2. Tuescher O, Protopopescu X, Pan H, Cloitre M, Butler T, Goldstein M, Root JC, Engelien A, Furman D, Silverman M, Yang Y, Gorman J, LeDoux J, Silbersweig D, Stern E. Differential activity of subgenual cingulate and brainstem in panic disorder and PTSD. J Anxiety Disord 2011; 25(2): 251–257
3. Goossens L, Leibold N, Peeters R, Esquivel G, Knuts I, Backes W, Marcelis M, Hofman P, Griez E, Schruers K. Brainstem response to hypercapnia: a symptom provocation study into the pathophysiology of panic disorder. J Psychopharmacol 2014; 28(5): 449–456
4. Sakai Y, Kumano H, Nishikawa M, Sakano Y, Kaiya H, Imabayashi E, Ohnishi T, Matsuda H, Yasuda A, Sato A, Diksic M, Kuboki T. Cerebral glucose metabolism associated with a fear network in panic disorder. Neuroreport 2005; 16(9): 927–931
5. Boshuisen ML, Ter Horst GJ, Paans AM, Reinders AA, den Boer JA. rCBF differences between panic disorder patients and control subjects during anticipatory anxiety and rest. Biol Psychiatry 2002; 52(2): 126–135
6. Iacono RP, Nashold BS Jr. Mental and behavioral effects of brain stem and hypothalamic stimulation in man. Hum Neurobiol 1982; 1(4): 273–279
7. Bertoglio LJ, de Bortoli VC, Zangrossi H Jr. Cholecystokinin-2 receptors modulate freezing and escape behaviors evoked by the electrical stimulation of the rat dorsolateral periaqueductal gray. Brain Res 2007; 1156: 133–138
8. Schenberg LC, Vasquez EC, da Costa MB. Cardiac baroreflex dynamics during the defence reaction in freely moving rats. Brain Res 1993; 621(1): 50–58
9. Schenberg LC, Bittencourt AS, Sudré EC, Vargas LC. Modeling panic attacks. Neurosci Biobehav Rev 2001; 25(7-8): 647–659
10. Moreira FA, Gobira PH, Viana TG, Vicente MA, Zangrossi H, Graeff FG. Modeling panic disorder in rodents. Cell Tissue Res 2013; 354(1): 119–125
11. Vargas LC, Schenberg LC. Long-term effects of clomipramine and fluoxetine on dorsal periaqueductal grey-evoked innate defensive behaviours of the rat. Psychopharmacology (Berl) 2001; 155(3): 260–268
12. Hogg S, Michan L, Jessa M. Prediction of anti-panic properties of escitalopram in the dorsal periaqueductal grey model of panic anxiety. Neuropharmacology 2006; 51(1): 141–145
13. Fogaça MV, Lisboa SF, Aguiar DC, Moreira FA, Gomes FV, Casarotto PC, Guimarães FS. Fine-tuning of defensive behaviors in the dorsal periaqueductal gray by atypical neurotransmitters. Braz J Med Biol Res 2012; 45(4): 357–365
14. Sergio TO, Spiacci A Jr, Zangrossi H Jr. Effects of dorsal periaqueductal gray CRF1- and CRF2-receptor stimulation in animal models of panic. Psychoneuroendocrinology 2014; 49: 321–330
15. Ullah F, Dos Anjos-Garcia T, Mendes-Gomes J, Elias-Filho DH, Falconi-Sobrinho LL, Freitas RL, Khan AU, Oliveira R, Coimbra NC. Connexions between the dorsomedial division of the ventromedial hypothalamus and the dorsal periaqueductal grey matter are critical in the elaboration of hypothalamically mediated panic-like behaviour. Behav Brain Res 2017; 319: 135–147
16. Graeff FG. Serotonin, the periaqueductal gray and panic. Neurosci Biobehav Rev 2004; 28(3): 239–259
17. Chen S, Zhou H, Guo S, Zhang J, Qu Y, Feng Z, Xu K, Zheng X. Optogenetics based rat-robot control: optical stimulation encodes "Stop" and "Escape" commands. Ann Biomed Eng 2015; 43(8): 1851–1864
18. Sandner G, Di Scala G, Rocha B, Angst MJ. *C-fos* immunoreactivity in the brain following unilateral electrical stimulation of the dorsal periaqueductal gray in freely moving rats. Brain Res 1992; 573(2): 276–283
19. Lim LW, Temel Y, Visser-Vandewalle V, Blokland A, Steinbusch H. Fos immunoreactivity in the rat forebrain induced by electrical stimulation of the dorsolateral periaqueductal gray matter. J Chem Neuroanat 2009; 38(2): 83–96
20. Thanos PK, Robison L, Nestler EJ, Kim R, Michaelides M, Lobo MK, Volkow ND. Mapping brain metabolic connectivity in awake rats with μPET and optogenetic stimulation. J Neurosci 2013; 33

(15): 6343–6349
21. Zhu Y, Xu K, Xu C, Zhang J, Ji J, Zheng X, Zhang H, Tian M. PET mapping for brain-computer interface stimulation of the ventroposterior medial nucleus of the thalamus in rats with implanted electrodes. J Nucl Med 2016; 57(7): 1141–1145
22. Zhu Y, Du R, Zhu Y, Shen Y, Zhang K, Chen Y, Song F, Wu S, Zhang H, Tian M. PET mapping of neurofunctional changes in a posttraumatic stress disorder model. J Nucl Med 2016; 57(9): 1474–1477
23. Mergenthaler P, Lindauer U, Dienel GA, Meisel A. Sugar for the brain: the role of glucose in physiological and pathological brain function. Trends Neurosci 2013; 36(10): 587–597
24. Volkow ND, Wang GJ, Telang F, Fowler JS, Goldstein RZ, Alia-Klein N, Logan J, Wong C, Thanos PK, Ma Y, Pradhan K. Inverse association between BMI and prefrontal metabolic activity in healthy adults. Obesity (Silver Spring) 2009; 17(1): 60–65
25. Bittencourt AS, Nakamura-Palacios EM, Mauad H, Tufik S, Schenberg LC. Organization of electrically and chemically evoked defensive behaviors within the deeper collicular layers as compared to the periaqueductal gray matter of the rat. Neuroscience 2005; 133(4): 873–892
26. McIntyre CC, Mori S, Sherman DL, Thakor NV, Vitek JL. Electric field and stimulating influence generated by deep brain stimulation of the subthalamic nucleus. Clin Neurophysiol 2004; 115(3): 589–595
27. LaLumiere RT. A new technique for controlling the brain: optogenetics and its potential for use in research and the clinic. Brain Stimul 2011; 4(1): 1–6
28. Menant O, Andersson F, Zelena D, Chaillou E. The benefits of magnetic resonance imaging methods to extend the knowledge of the anatomical organisation of the periaqueductal gray in mammals. J Chem Neuroanat 2016; 77: 110–120
29. Vianna DM, Brandão ML. Anatomical connections of the periaqueductal gray: specific neural substrates for different kinds of fear. Braz J Med Biol Res 2003; 36(5): 557–566
30. Sébille SB, Belaid H, Philippe AC, André A, Lau B, François C, Karachi C, Bardinet E. Anatomical evidence for functional diversity in the mesencephalic locomotor region of primates. Neuroimage 2017; 147: 66–78
31. Chakravarthy VS, Joseph D, Bapi RS. What do the basal ganglia do? A modeling perspective. Biol Cybern 2010; 103(3): 237–253
32. Sillery E, Bittar RG, Robson MD, Behrens TE, Stein J, Aziz TZ, Johansen-Berg H. Connectivity of the human periventricular-periaqueductal gray region. J Neurosurg 2005; 103(6): 1030–1034
33. Moers-Hornikx VM, Vles JS, Lim LW, Ayyildiz M, Kaplan S, Gavilanes AW, Hoogland G, Steinbusch HW, Temel Y. Periaqueductal grey stimulation induced panic-like behaviour is accompanied by deactivation of the deep cerebellar nuclei. Cerebellum 2011; 10(1): 61–69
34. Stark-Inbar A, Dayan E. Preferential encoding of movement amplitude and speed in the primary motor cortex and cerebellum. Hum Brain Mapp 2017; 38(12): 5970–5986
35. Garakani A, Buchsbaum MS, Newmark RE, Goodman C, Aaronson CJ, Martinez JM, Torosjan Y, Chu KW, Gorman JM. The effect of doxapram on brain imaging in patients with panic disorder. Eur Neuropsychopharmacol 2007; 17(10): 672–686
36. Sobanski T, Wagner G. Functional neuroanatomy in panic disorder: status quo of the research. World J Psychiatry 2017; 7(1): 12–33
37. Bisaga A, Katz JL, Antonini A, Wright CE, Margouleff C, Gorman JM, Eidelberg D. Cerebral glucose metabolism in women with panic disorder. Am J Psychiatry 1998; 155(9): 1178–1183
38. Bernal-Casas D, Lee HJ, Weitz AJ, Lee JH. Studying brain circuit function with dynamic causal modeling for optogenetic fMRI. Neuron 2017; 93(3): 522–532.e5